J Porous Mater (2008) 15:419–425
DOI 10.1007/s10934-007-9101-y

Synthesis of porous biomorphic α/β-Si_3N_4 composite from sea sponge

C. R. Rambo · H. Sieber · L. A. Genova

Received: 25 July 2006 / Revised: 17 November 2006 / Published online: 12 May 2007

Abstract Biomorphic α/β-Si_3N_4 composites were produced from natural sea sponge via replication method. The sponges were impregnated with a Si-containing slurry via dip-coating. After coating, the sponges were submitted to oxidation at 600°C for 1 h to decompose the bio-polymers followed by burning out of carbon, leading to a Si-skeleton. Subsequent thermal treatment at 1,450°C for 5 h under flowing nitrogen promoted the nitridation of the Si resulting in α/β-Si_3N_4 with an α/β fraction of 67%. The ceramic composite maintained the original morphology of the sea sponge and exhibited a porosity of 88%. The microstructure comprised whiskers, small irregular shaped particles and rod-like hexagonal grains.

Keywords Biomorphic ceramics · Porous Si_3N_4 · Dip-coating · Nitridation

C. R. Rambo (✉)
Group of Ceramic and Glass Materials—CERMAT, Department of Chemical Engineering—EQA/UFSC, Federal University of Santa Catarina, P.O. Box 476, Florianopolis 88040-900 SC, Brazil
e-mail: rambo@enq.ufsc.br

H. Sieber
Department of Materials Science, Glass and Ceramics, University of Erlangen-Nuremberg, Martensstrasse, 5, 91058 Erlangen, Germany

L. A. Genova
Center of Materials Science and Technology, Energy and Nuclear Research Institute, Av. Lineu Prestes, 2242, Cidade Universitária, Sao Paulo, SP 05588-900, Brazil

1 Introduction

1.1 Silicon nitride ceramics

Silicon nitride is a very interesting structural ceramic due to its excellent properties, such as high fracture toughness, low thermal expansion coefficient (3×10^{-6} per °C), high strength at high temperatures, high elastic modulus (320 GPa), and high corrosion resistance [1, 2]. These properties make Si_3N_4 ceramics potential candidates for applications at severe conditions [3].

Two well-known crystal structures of silicon nitride are of engineering interest: α-Si_3N_4 and β-Si_3N_4. The mechanical properties of silicon nitride-based-ceramics are strongly dependent on their microstructure. It is well know that the presence of large, elongated β-Si_3N_4 grains with high aspect ratio enhances the toughness, by deflecting the propagation of cracks. However, for the toughness mechanisms to be effective, the energy of the grain/liquid interface should be adapted and in that way the composition of the liquid phase (and therefore, of the sintering additives) is decisive [4–8]. The developed microstructure of the silicon nitride is directly related to the α/β ratio in the raw material, to the composition of the sintering additives, and to the applied sintering method [4, 9].

Silicon nitride can be fabricated by different methods, such as hot pressing, hot isostatic pressing, pressure less sintering or direct nitridation of Si-powder (reaction bonding). The direct nitridation of metallic Si was one of the first methods to produce Si_3N_4 powders as well as solid parts (reaction-bonded silicon nitride) and it is still the most commonly used processes to produce silicon nitride with low cost raw materials and low processing temperatures [10–13]. This method allows near-net shaping of complex structures.

Although direct nitridation is a relatively simple and inexpensive process, the quality of the produced powder is difficult to control, particularly with respect to the α/β phase ratio. The powder usually contains about 92% of α-Si_3N_4 [14], which is considered as not desirable for many applications. The formation of the α-phase occurs between 1,200 and 1,400°C, with its kinetic increasing with temperatures up to close to the upper limit. On the other hand, as the melting temperature of Si (1,410°C) is very close to this limit and considering that the presence of a liquid phase favors the β-phase formation, the exothermic character of the reaction acquires a rigid control of the reaction temperature, which is fundamental to control the relation of the formed α/β phases.

1.2 Cellular ceramics

In the recent years the interest in porous materials with cellular structures, such as foams, reticulated and biomorphic materials has increased due to their specific properties such as low density, low thermal conductivity, thermal stability, high-surface area, and high permeability [15–17]. These properties make porous ceramics suitable for a wide range of technological applications, including, catalyst supports, filters for molten-metals and hot gases, thermal insulators, refractory linings, and biomaterials [18, 19]. Various processing routes have been proposed for production of porous ceramics, including polymeric sponge [20–22] and direct foaming and foaming agents [23, 24]. The fabrication method determines the range of porosity, the pore size distribution, and the pore morphology. The polymeric sponge method [20] is a simple, inexpensive and versatile way for producing ceramic foams. This method consists in the impregnation of a polymeric sponge with slurries containing appropriate binders, followed by a heat-treatment to burn out the organic template (foam) and to sinter the remaining skeleton.

The anatomical features of naturally grown materials are an attractive template for the design of porous cellular ceramics and ceramic composites, where the morphology of the native tissue is maintained in the ceramic product [25–27]. The main innovative characteristic of this methodology is the possibility to design macro- and microcellular parts, which could not be produced by other conventional techniques. In the recent years, different biotemplating technologies were developed for the conversion of biological templates such as wood, cellulosic and fibrous materials into biomorphic ceramics [27].

The previous work on biotemplating was mainly focused on the manufacturing of biomorphic carbide and oxide-based ceramics from natural lignocellulosic structures by different reactive processing routes. The synthesis can be generally distinguished by the way of incorporating precursors into the in natura or carbonized biological template, e.g., metal melt [28] or vapor infiltration [29–31], sol-gel process [32–35], dip-coating of metal/ceramic or pre-ceramic polymers [36–38].

Up to now, there is no established processing technology for manufacturing of cellular nitride ceramics. The polymeric sponge method requires a carbon-based template to produce the sponge. The burning out of carbon leads to a powder skeleton that collapses during handle. This work reports a one-step process to obtain cellular biomorphic Si_3N_4 ceramics. The replication method is applied using an oxidation–nitridation process.

2 Experimental

The biomorphic Si_3N_4 sponges were prepared by the replication method. An open-porous, natural sea sponge (*Hippiospongia Lachne*) was used as starting material for the preparation of the porous Si_3N_4 sponges. The sponge anatomy is characterized by regular cells formed by elongated struts. Typical diameters of the cells range from 200 to 250 μm. The cells form a network, which give rise for large interconnected pores with sizes ranging from 1 to 3 mm, Fig. 1.

The sponge was cut in samples of ~$3 \times 3 \times 3$ cm^3, dried at 130°C for 2 h in air and infiltrated by dip-coating with a metallic Si-slurry. The slurry was prepared with isopropyl alcohol containing 80 vol.% Si-powder (>98%) and 5 vol.% bakelite as binder. The infiltrated sponges were oxidized at 600°C for 30 min to decompose the bio-polymeric chains and to burn out the carbon, leading to a fragile Si-skeleton and subsequently nitrided at 1,450°C for 5 h in flowing pure N_2 atmosphere (1.5 l/min). No sintering aids were used.

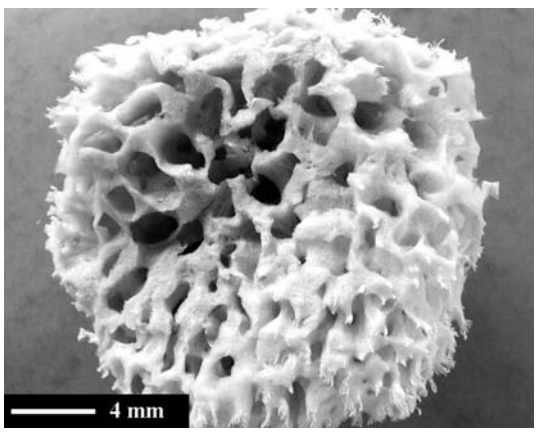

Fig. 1 Digital photograph of the natural sponge (*Hippiospongia Lachne*)

Thermogravimetric analyses (TGA) was applied to evaluate the weight gain of the Si-infiltrated sponges during oxidation (Du Pont Thermo Analyze, 951, Paris, France). The phase composition of the ceramized sponge was determined by X-ray diffractometry (XRD) (Siemens D 500, Munich, Germany) working with monochromated CuK_{α} radiation. The microstructure was characterized by scanning electron microscopy (SEM) (FEI, Quanta 200, Brno, Czech Republic). The skeleton density was measured by He-pycnometry (Micromeritics, Accu Pyk 1330, Neuss, Germany). The open porosity was estimated by the relation between the skeleton and the geometrical densities. Micro-computer tomography (μCT) operating at 40 kV and 80 μA at a wave length of 0.024 nm was applied to characterize the cellular microstructure of the biomorphous ceramic sponges. The specimens were scanned in a near isotropic resolution of $37 \times 37 \times 38$ μm^3. A CCD line array was used to detect the transmitted intensity through the sample. X-ray source and detector were covered with slit collimators. The object was rotated over 360° with one step per degree and the raw data were recorded as sinugrams. A more detailed description of foam structure characterization by μCT was reported by Zeschky et al. [39].

The strength under compression of a set of three samples with nominal dimensions of $7.5 \times 7.5 \times 0.5 \pm 0.1$ mm^3 was determined at room temperature using an universal testing device (Instron, Model 4202, Instron Corp., Canton, MA, USA). The speed of the crosshead was set constant to 1 mm/min. Representative dense parts (excluding the large pores) of the samples were cut and prepared for the mechanical tests.

3 Results and discussion

Figure 2 shows the TGA curve of the Si-powder up to 1,100°C in air. Up to 600°C, only a minor weight gain due to start of the oxidation is observed (~0.9 wt.%). The temperature of 600°C was chosen as the oxidation temperature because all carbon is already oxidized [35] and a minor oxidation occurs on the Si-surface.

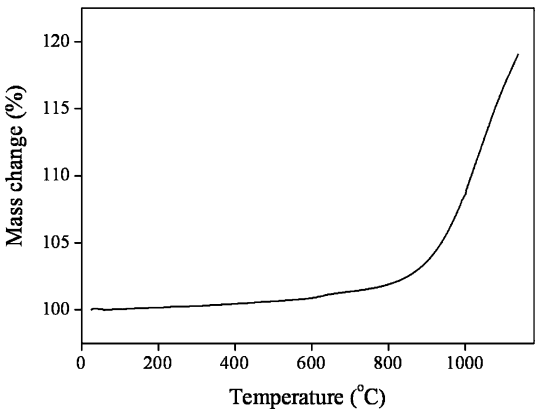

Fig. 2 Thermogravimetric curve of silicon powder up to 1,100°C at 10°C/min in air

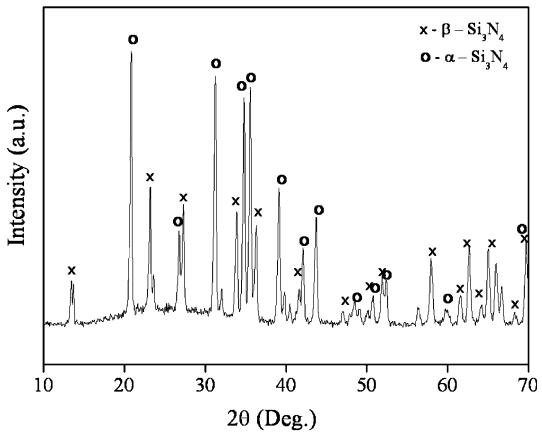

Fig. 3 X-ray diffractogram of the biomorphic sponge after nitridation

3.1 Phase evaluation

Figure 3 shows the X-ray diffraction pattern of the ceramic product after nitridation. The diffraction peaks related to β (JCPDS: 33-1160) and α (JCPDS: 09-0250) phases of Si_3N_4 indicates a full conversion of the Si into Si_3N_4. Among the possible reactions that may form Si_3N_4, direct nitridation of metallic Si was the dominant reaction:

$$3Si + 2N_2 \rightarrow Si_3N_4 \ \Delta G_o^{1,450^{\circ}C} = -173.4 \text{ KJ/mol.} \quad (1)$$

The diffusion mechanism for further formation of Si_3N_4 during nitridation of Si is extensively discussed in the literature [40–43]. Zhu et al. [44] synthesized Si_3N_4 on Si-wafers using pure flowing N_2 at 1,100°C. Once the first Si_3N_4 layer is formed on the Si-surface, N_2 diffuses through the Si/Si_3N_4 to form subsequent Si_3N_4 layers [41].

No Si or SiC was detected by XRD. The absence of SiC phases can be related to the low reaction temperature, which favored the oxidation of carbon into CO prior than SiC formation. Also, the flowing N_2 allows the rapid escape of the CO formed from the sample, further promoting the formation of Si_3N_4 prior to the formation of SiC [45]. Additionally, carbothermal reduction of surface SiO_2 by carbon residue with subsequent nitridation under normal (room) conditions is thermodynamically impossible at 1,450°C as shows Eq. 2 [45]:

$$3SiO_2 + 6C + 2N_2 \rightarrow Si_3N_4 + 6CO \ \Delta G_o^{1,450} = 20.1 \text{ KJ/mol.} \quad (2)$$

This reaction starts to be thermodynamically possible at temperatures above 1,475°C ($\Delta G_o^{1,477^{\circ}C}$ = -0.3 KJ/mol).

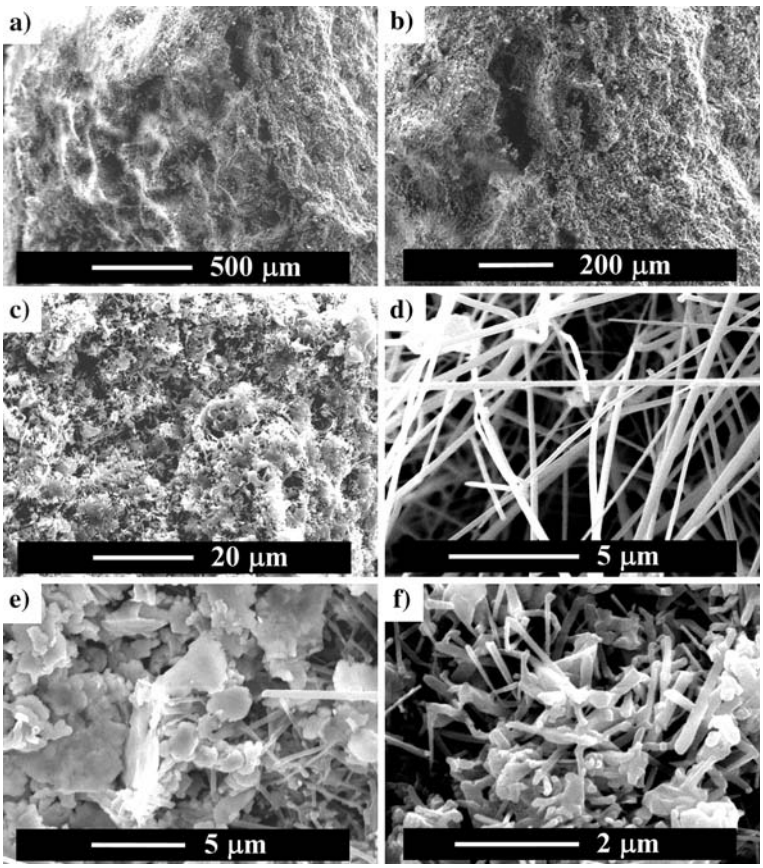

Fig. 4 SEM micrographs of the biomorphic Si_3N_4 sea sponge with different magnitudes

Beside the native oxide layer on the Si surface, thermal oxidation of silicon is achieved by heating the substrate to temperatures typically higher than 800°C in oxidative atmosphere. As the specimen was first exposed only to an oxidation process at 600°C, it is not expected the Si-particles to exhibit a thick SiO_2 layer in their surface, which could decrease the reaction rate or even hinder the Si_3N_4 formation.

The relative β/α fraction was estimated using the relation between the intensities of the (210) diffractions of both phases, according to Gazzara and Messier [46]:

$$\phi_\beta = \frac{I_\beta^{(210)}}{I_\beta^{(210)} + I_\alpha^{(210)}}. \quad (3)$$

A relative fraction of 33% of the β-phase was obtained, indicating the predominance of α-Si_3N_4 after 5 h at 1,450°C. During the early stages of nitridation at temperatures lower than 1,400°C the formation of α-Si_3N_4 is dominant. As the nitridation temperature and time increase, the relative β-Si_3N_4 fraction increases [42]. The fundamental difference between α- and β-Si_3N_4 formation is that α-Si_3N_4 results from silicon complexing with molecular nitrogen and the latter results from complexing with essentially atomic nitrogen [40]. Most surface reaction produces α-Si_3N_4, which is explained by the removal of active (atomic) nitrogen by oxygen. N_2 will diffuse by Knudsen diffusion and form β-phase in the inner Si-layers [42]. Besides the reaction mechanisms involved, the surface area or free reaction surface is also an important factor to take into account. Due to the high porosity and relatively high surface area of the Si-infiltrated sponge template, the α-Si_3N_4 reaction was preferentially dominant, leading to a phase mixture with relatively high α/β fraction [40].

3.2 Microstructure and macro-morphology

Figure 4 shows SEM micrographs of the Si_3N_4 sponge. Large voids surrounded by relatively dense ceramic walls confirm the reproduction of the anatomy of the sea sponge (Fig. 4a). Pores with sizes varying from 50 to 200 µm form the pore network of the Si_3N_4 sponge (Fig. 4b).

The microstructure of the biomorphous Si_3N_4 is shown in Fig. 4c–f. Si_3N_4 elongated grains of low aspect ratio are embedded in a matrix composed by particles with sizes in the range of 1–5 µm. Long α-Si_3N_4 whiskers are also distributed within the interparticle spaces (Fig. 4c, d). The whiskers exhibit widths of 500 nm in average and high

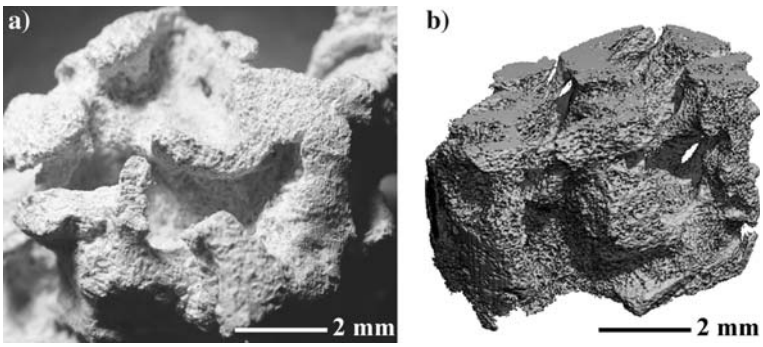

Fig. 5 Macromorphology of the biomorphic Si_3N_4 sponge: a Digital photograph; b Reconstructed 3D image obtained from micro-computer tomography

aspect ratios (higher than 20) were formed by a vapor–liquid–solid mechanism (VLS), where Si-vapor reacts with molecular nitrogen at the surface, forming the first Si_3N_4 layers as discussed in the last section. Furthermore, as no sintering additive was used, the SiO_2 formed after oxidation could promote the coarsening of the width and shortening of the length of the Si_3N_4 grains [45]. At 1,450°C, typical elongated hexagonal β-Si_3N_4 grains with widths in the range of 0.1–0.5 μm were formed, resulting in a porous interconnected fibrous network (Fig. 4e, f).

Figure 5 shows comparatively a photograph (Fig. 5a) and a μCt image (Fig. 5b) of the biomorphic Si_3N_4 sponge. The macropores (around 2–3 mm) of the sea sponge were well reproduced in the Si_3N_4 ceramics. The porous struts are also visible in the macro photograph. The μCT analysis built with a relatively good accuracy the macrostructure of the biomorphic Si_3N_4 ceramic, as can be seen in Fig. 5b.

Table 1 summarizes the microstructural properties of the biomorphic Si_3N_4 sponge, derived from He-pycnometry and μ-CT analysis.

The connectivity density (CD) was computed from CT data using the ConnEulor principle as explained in detail in [47, 48]. Reconstructed two-dimensional CT data images of two neighbored slices are compared by the Boolean ''Exclusive-Or'' operator. The result is superimposed to the original pictures and analyzed. All new connections (B), holes (H) and islands (I) are counted and CD is calculated by:

$$\mathrm{CD} = -\frac{\sum H + \sum I - \sum B}{2h \cdot A}, \qquad (4)$$

Table 1 Physical properties of the biomorphic Si_3N_4

	Biomorphic Si_3N_4
ρ_{rel} (g/cm^3)	0.225 ± 0.005
ρ_{strut} (g/cm^3)	2.62 ± 0.05
Porosity (%)	88 ± 1
CD (1/mm^3)	71.32
Anisotropy	1.11 ± 0.05
Compressive strength (MPa)	31 ± 5

ρ_{rel} relative density, *CD* connectivity density, ρ_{strut} strut density

where h is the distance of the two slices (h = 38 μm) and A the examined image area. In the case of determining the CD of the pores, B and I denote cell windows and cells, respectively. The value is identical if CD is calculated for the strut material, where B denotes new struts, H equal cells and I isolated struts, respectively. Compared with other μ-CT analysis of different scaffolds presented in the literature [31, 49], the biomorphic Si_3N_4 sponge exhibits a low degree of anisotropy (close to 1) and a high connectivity density (above 70 mm^{-3}).

The strut density of the biomorphic Si_3N_4 sponge is 2.62 g/cm^3, which is lower than the theoretical density of hot pressed Si_3N_4 (3.1–3.3 g/cm^3), but in the range of the RBSN (2.3–2.7 g/cm^3). The relative density is very low (0.22) and hence the biomorphic Si_3N_4 sponge exhibit a total porosity of 88%. Direct nitridation of Si produces only a small volume change in the samples [42], which explains the fact that no visible shrinkage occurred after the process.

3.3 Mechanical properties

Figure 6 shows the compressive stress-strain curves of the biomorphous Si_3N_4 derived from sea sponge.

Gibson and Ashby [50] developed a generic model to explain the failure mechanism in cellular solids (honeycombs and foams). In the case of brittle foams like

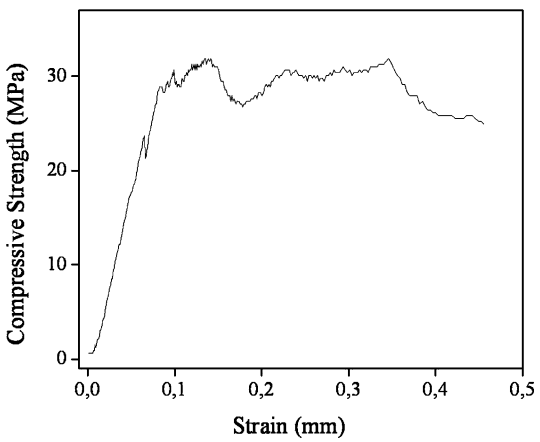

Fig. 6 Strength under compression of the biomorphic Si_3N_4 sponge

ceramics and glasses, they collapse by brittle crushing. Three basic stages in the stress-strain curve of brittle foams are relevant. They exhibit a linear elastic deformation, characterized by a critical stress (maximum), followed by a long collapse plateau (cells crashing at a constant stress). This plateau is truncated by a densification process, when the cell walls touch each other (stress increasing). The biomorphic Si_3N_4 bodies appear to fail by catastrophic collapse of the cells, as predicted by Gibson–Ashby, in which the three distinct stages are observed. The whole porous sample can be described as a cellular material with different cell geometries formed by the fibrous network. A mean strength under compression of 31 MPa was obtained. Although the biomorphous α/β-Si_3N_4 exhibits high porosity, this strength is relatively high compared to other porous Si_3N_4. Fine fibrous β-grains contributes to the strength and elongated, coarser β-grains enhance the fracture toughness [51, 52].

4 Conclusions

Biomorphic Si_3N_4 sponges were produced by replication of natural sea sponge. Nitridation of silicon skeleton at 1,450°C resulted in the formation of both β- and α-Si_3N_4 phases, where the α-phase was the majority one. The final biomorphic ceramic maintained the original anatomy of the sea sponge down to the micrometer level. A high strength under compression was achieved despite the relatively high porosity.

Highly porous, light weight α/β-Si_3N_4 composites with a good mechanical strength are potentially useful for applications in medicine as scaffold structures or as porous support for catalysts. Fibrous like α/β-Si_3N_4 composites may be also useful for applications in hot gas filtration systems.

Acknowledgments The authors thank CNPq-Brazil. The Volkswagen Foundation is also thankfully acknowledged for the financial support under contract I/73 043.

References

1. D.R. Lide, *CRC Handbook of Chemistry and Physics*, 76th edn (CRC, Boca Raton, 1995)
2. F.L. Riley, J. Amer. Ceram. Soc. **83**, 245 (2000)
3. K.H. Jack, Mater. Sci. Forum **325–326**, 255 (2000)
4. G.E. Petzow, Microstruct Sci **23**, 3 (1995)
5. G. Petzow, M. Hermann, in High Performance Non-Oxide Ceramics II, ed. by M. Jansen (Springer, Berlin, 2002), p. 47
6. S. Hampshire, in Materials Science and Technology—A Comprehensive Treatment, ed. by M.V. Swain (VCH, Weinheim, 1995), p. 121
7. F.F. Lange, Int. Metals Rev. **247**, 1 (1980)
8. J. Marchi, J.C. Bressiani, A.H.A. Bressiani, Key Eng. Mat. **189**, 120 (2001)
9. J. Dualibi Fh., J.C. Bressiani, Mater. Sci. Eng. A **209**, 164 (1996)
10. R.G. Pigeon, A. Varma, A.E. Miller, J. Mater. Sci. **28**, 1919 (1993)
11. R.G. Pigeon, A. Varma, J. Mater. Sci. **28**, 2999 (1993)
12. B.T. Lee, H.D. Kim, Mater. Sci Eng. A **364**, 126 (2004)
13. K.A. Appiagyei, Key Eng. Mat. **224–226**, 309 (2002)
14. D.L. Segal, Chem. Ind. **16**, 544 (1985)
15. P. Colombo, E. Bernardo, Composites Sci. Tech. **63**, 2353 (2003)
16. P. Ciambelli, V. Palma, P. Russo, S. Vaccaro, Catal. Today **75**, 471 (2002)
17. M.D.M. Innocentini, A.R.F. Pardo, B.A. Menegazzo, L.R.M. Bittencourt, R.P. Rettore, V.C. Pandolfelli, J. Am. Ceram. Soc. **85**, 1517 (2002)
18. P. Sepulveda, Am. Ceram. Soc. Bull. **76**, 61 (1997)
19. L. Montanaro, Y. Jorand, G. Fantozzi, A. Negro, J. Eur. Ceram. Soc. **18**, 1339 (1998)
20. K. Schwartzwalder, A.V. Somers, *Method of making porous ceramics articles* (US Pat. No. 3 090 094, May 21, 1963)
21. J. Saggio-Woyansky, C.E. Scottetal, Amer. Ceram. Soc. Bull. **71**, 1674 (1992)
22. E. Sousa, C.B. Silveira, T. Fey, P. Greil, D. Hotza, A.P.N. Oliveira, Adv. Appl. Ceram. **104**, 22 (2005)
23. P. Sepulveda, J.G.P. Binner, J. Eur. Ceram. Soc. **19**, 2059 (1999)
24. H.X. Peng, Z. Fan, J.R.G. Evans, J.J.C. Busfield, J. Eur. Ceram. Soc. **20**, 807 (2000)
25. A.H. Heuer, D.J. Fink, V.J. Arias, P.D. Calvert, K. Kendali, G.L. Messing, J. Blackwell, P.C. Rieke, D.H. Thompson, A.P. Wheeler, A. Veis, A.I. Caplan, Science **255**, 1098 (1992)
26. C.E. Byrne, D.E. Nagl, Mat. Res. Innovat. **1**, 137 (1997)
27. H. Sieber, Mat. Sci Eng A **412**, 43 (2005)
28. P. Greil, T. Lifka, A. Kaindl, J. Eur. Ceram. Soc. **18**, 1961 (1998)
29. E. Vogli, H. Sieber, P. Greil, J. Eur. Ceram. Soc. **22**, 2663 (2002)
30. C.R. Rambo, H. Sieber, Adv. Mater. **17**, 1088 (2005)
31. C.R. Rambo, F.A. Mueller, L. Mueller, H. Sieber, I. Hofmann, P. Greil, Mater. Sci. Eng. C **26**, 92 (2006)
32. C.R. Rambo, J. Cao, O. Rusina, H. Sieber, Carbon **43**, 1174 (2005)
33. T. Ota, M. Takahashi, T. Hibi, M. Ozawa, S. Suzuki, Y. Hikichi, J. Am. Ceram. Soc. **78**, 3409 (1995)
34. M. Patel, B.K. Padhi, J. Mat. Sci. **25**, 1335 (1990)
35. J. Cao, C.R. Rambo, H. Sieber, J. Porous Mater. **11**, 163 (2004)
36. H. Sieber, A. Kaindl, D. Schwarze, J.-P. Werner, P. Greil, cfi/Ber. DKG **77**, 21 (2000)
37. H. Sieber, D. Schwarze, F. Mueller, P. Greil, in Advanced Ceramics, Materials, and Structures: B, ed. by M. Singh, T. Jensen (The American Ceramic Society, Westerville, OH, 2001), p. 225
38. C.R. Rambo, H. Sieber, J. Mater. Sci. **41**, 3315 (2006)
39. J. Zeschky, T. Hoefner, C. Arnold, R. Weihmann, D. Bahloul-Hourlier, M. Scheffler, P. Greil, Acta Mater. **53**, 927 (2005)
40. H.M. Jennings, J. Mater. Sci. **18**, 951 (1983)
41. F.-W. Chang, T.-H. Liou, F.-M. Tsai, Thermochimica Acta **354**, 71 (2000)
42. B. Lei, O. Babushkin, R. Warren, J. Eur. Cer. Soc. **17**, 1113 (1997)
43. W.B. Li, B.Q. Lei, T. Lindbäk, J. Eur Ceram. Soc. **17**, 1119 (1997)
44. H. Zhu, D. Yang, L. Wang, D. Due, Thin Solid Films **474**, 326 (2005)
45. J.-F. Yang, S.-Y. Shan, R. Janssen, G. Schneider, T. Ohji, S. Kanzaki, Acta Mater. **53**, 2981 (2005)
46. C. Gazzara, D. Messier, Am. Ceram. Soc. Bull. **56**, 777 (1977)
47. T. Hildebrand, R. Rüegsegger, J. Microsc. **185**, 67 (1997)

48. H.J.G. Gundersen, R.W. Boyce, J.R. Nyengaard, A. Odgaard, Bone **14**, 217 (1993)
49. A.C. Jones, B. Milthorpe, H. Averdunk, A. Limaye, T.J. Senden, A. Sakellariou, A.P. Sheppard, R.M. Sok, M.A. Knackstedt, A. Brandwood, D. Rohner, D.W. Hutmacher, Biomaterials **25**, 4947 (2004)
50. L.J. Gibson, M.F. Ashby, *Cellular Solids: Structure and Properties*, 2nd edn (Cambridge University Press, Cambridge, 1997)
51. M.J. Hoffmann, G. Petzow, Pure Appl. Chem. **66**, 1807 (1994)
52. M.J. Hoffmann, Pure Appl. Chem. **67**, 939 (1995)